J. Fluid Mech. (2009), *vol.* 640, *pp.* 109–129.
doi:10.1017/S0022112009991285

Momentum and heat transport in a three-dimensional transitional wake of a heated square cylinder

L. DJENIDI† AND R. A. ANTONIA

Discipline of Mechanical Engineering, School of Engineering, University of Newcastle, Newcastle 2308 NSW, Australia

(Received 26 March 2009; revised 19 July 2009; accepted 19 July 2009; first published online 27 October 2009)

The transport of momentum and a passive scalar (temperature) in a three-dimensional transitional wake of a heated square cylinder has been carried out through direct numerical simulations using the lattice Boltzmann method at a Reynolds number $R_d = 200$ (d is the cylinder diameter) and a Prandlt number of 0.7. The simulations shows that while momentum and heat are transported by vortical structures, heat is in general more effectively transported than momentum. It is argued that the nature of the structural flow is responsible for the longitudinal heat flux $\overline{u\theta}$ being larger than the lateral one $\overline{v\theta}$ in the wake region extending up to $45d$. It was shown that a gradient transport model could, to a first-order approximation, be used to model $\overline{uv}$ but would be less accurate for modelling $\overline{v\theta}$. Also the Reynolds analogy between momentum and heat transports is not verified in this flow. The fluctuating temperature field presents thermal structures similar to the velocity structures with, however, a different spatial organization. In addition the analogy between fluctuating turbulent kinetic energy and the temperature variance is relatively well satisfied throughout the wake flow.

1. Introduction

Antonia & Mi (1993) presented analytical solutions for the vorticity and temperature fields in an infinitely long axisymmetric line vortex diffusing into the surrounding (ambient temperature) fluid (here and in the rest of the paper temperature is considered as a passive scalar with no dynamic effect on the fluid flow). They assumed that both the temperature and vorticity follow the same transport equation:

$$\frac{\partial \xi}{\partial t} = \frac{A_\xi}{r}\frac{\partial}{\partial r}\left(r\frac{\partial \xi}{\partial r}\right), \tag{1.1}$$

where ξ represents either the vorticity or temperature, A_ξ is a constant (equal to either the fluid kinematic viscosity or the thermal diffusivity) and r is the radial distance from the centre of the vortex. They obtained the following distribution form for the two quantities:

$$\xi = \frac{\beta_\xi}{t}\mathrm{e}^{-r^2/\alpha_\xi t}, \tag{1.2}$$

† Email address for correspondence: lyazid.djenidi@newcastle.edu.au

where β_ξ and α_ξ $(=4A_\xi)$ are constant; the former is determined at time $t=0$. Earlier experimental verification of (1.2) for the vorticity was observed by Okude & Matsui (1987a) using both hot-wire and visualization techniques and by Green & Gerrard (1991) using optical interferometry. Also using hot wires, Okude & Matsui (1987b) measured the vorticity distribution in a cylinder wake ($R_d=140$) and found it to be in reasonable agreement with (1.2). Mi & Antonia (1994), using also hot-wire measurements in a wake cylinder ($R_d=98$), verified (1.2) for the vorticity. In addition, by carrying out cold-wire measurements for the same flow conditions but with a slightly heated cylinder, these latter authors provided an experimental verification of (1.2) for the temperature, confirming that temperature and vorticity behaved in similar fashion within a two-dimensional isolated vortex (see also Ezersky *et al.* 2000). From a practical point of view, this is very useful since temperature measurements can be made more reliably than vorticity measurements. Furthermore, verification of (1.2) for both vorticity and temperature is useful for the purpose of modelling thermal laminar vortices and using temperature as a relatively accurate marker of the vortices.

Godard (2001), Paranthoën *et al.* (2004) and Godard *et al.* (2005) studied the diffusion of temperature in a periodic laminar wake of a circular cylinder at a Reynolds number of 65. They introduced a heated line source in the near-wake and measured the velocity and temperature using laser Doppler anemometry (LDA) and cold-wire thermometry. They showed that the velocity field in the wake is strongly related to the geometric structure of vortices while the temperature field is controlled both by the time scale of rotation of the vortices and the location of the heated fluid within the vortex street. Furthermore, they observed that in the central part of the thermal plume, the transverse heat flux and transverse mean temperature gradient had always the same sign, which indicated that a gradient transport model (GTM) for heat was not appropriate to model heat transfer in this particular flow.

In the present paper, we investigate the transport of momentum and heat in a three-dimensional transitional wake of a slightly heated square cylinder. The motivation of the study stems in part from the fact that, as pointed out above, this aspect has to date received little attention. It is important to document how momentum and heat (or any passive scalar) are transported in transitional flows and in particular to determine the role of the velocity field in the transport of heat. Another reason for this work is related to the anomalous behaviour of the small-scale temperature field in turbulent flows (Sreenivasan 1996; Mydlarski & Warhaft 1998; Warhaft 2000; Watanabe & Gotoh 2004). This behaviour is associated with the ramp-cliff structures, which results from the converging and diverging separatrices and saddle points formed by large-scale velocity structures (Antonia *et al.* 1986; Matsumura & Antonia 1993). Watanabe & Gotoh (2004) showed that ramp-cliff structures exist whether or not a mean temperature gradient is present. Quite interestingly, Godard (2001) presented temperature signals, measured in a cylinder wake at $R_d=65$ (a heat line source was used to generate the passive scalar), which exhibited features similar to those associated with ramp-cliff signals. Since large-scale structures, through the ramp-cliff structures, play a significant role in the context of the small-scale anisotropy of the scalar field, the study of the temperature field in a three-dimensional transitional flow should provide useful insight in the general problem of scalar mixing. The three-dimensional transitional wake is interesting as it offers the possibility to follow the temperature behaviour from a (pseudo-)two-dimensional laminar environment to a three-dimensional pseudo-turbulent one. This makes it possible to investigate the effect of the velocity on the temperature field at different stages of the wake.

2. Numerical procedure

2.1. *Lattice Boltzmann method*

A direct numerical simulation (DNS) is carried out using the lattice Boltzmann method (LBM). Rather than solving the governing fluid equations (Navier–Stokes equations), the LBM solves the Boltzmann equation on a lattice. The basic idea of the LBM is to construct a simplified kinetic model that incorporates the essential physics of microscopic average properties, which obey the desired (macroscopic) Navier–Stokes equations (Frisch, Hasslacher & Pomeau 1986). With a sufficient amount of symmetry of the lattice, the LBM implicitly solves these latter equations with second-order accuracy. For the present calculations, each computational node consists of a three-dimensional lattice composed of 18 moving particles and a rest particle (lattice model D3Q19, for a developed account of LBM and its applications see Benzi, Succi & Vergassola 1992; Chen & Doolen 1998; Succi 2001; Djenidi 2006).

The standard lattice Boltzmann equation (LBE) with the Bhatnagar–Gross–Krook (BGK) approximation governing the time and space variations of the single-particle distribution $f_i(\boldsymbol{x}, t)$ at the lattice site $\boldsymbol{x}$ is

$$f_i(\boldsymbol{x} + \boldsymbol{e}_i \Delta t, t + \Delta t) - f_i(\boldsymbol{x}, t) = -\frac{1}{\tau}(f_i(\boldsymbol{x}, t) - f_i^{eq}(\boldsymbol{x}, t)), i = 0, 1, \ldots, 18, \qquad (2.1)$$

where τ is the relaxation time, Δt the time step, $\boldsymbol{e}_i$ $(= \Delta \boldsymbol{x}/\Delta t)$ is the particle velocity in the i-direction and f_i^{eq} is the equilibrium single-particle distribution:

$$f_i^{eq} = \rho \omega_i \left(1 + 3(\boldsymbol{e}_i \cdot \boldsymbol{u}) + \frac{9}{2}(\boldsymbol{e}_i \cdot \boldsymbol{u})^2 - \frac{3}{2}u^2\right), \qquad (2.2)$$

where $\rho(= \sum_i f_i)$ is the fluid density, $\boldsymbol{u}$ $(\rho \boldsymbol{u} = \sum_i f_i \boldsymbol{e}_i)$ is the local fluid velocity vector and ω_i are the corresponding weights ($\omega_i = 1/3$ for $i = 0$, $\omega_i = 1/18$ for $i = 1-6$ and $\omega_i = 1/36$ for $i = 7-18$; $i = 0$ corresponds to the rest particle in the centre of the cubic lattice, $i = 1, \ldots, 6$ correspond to the particles on the axis aligned with x, y and z, and $i = 7, \ldots, 18$ are related to the particles on the diagonal directions.)

The motivation for the choice of the LBM over the classical resolution of the Navier–Stokes equations has been presented in Djenidi (2006) and Djenidi & Moghtaderi (2006). We briefly summarize the reasons here: (i) extreme ease of implementing solid surfaces, (ii) no need for solving the Poisson equation for the pressure and (iii) ease of parallelizing the computations, which follows in part from (ii) and the fact the collision step is local in nature.

2.2. *Thermal lattice Boltzmann method*

A passive scalar approach (Massaioli, Benzi & Succi 1993; Yuan & Schaefer 2006) is implemented to compute the temperature field. In this approach the temperature satisfies the passive-scalar equation

$$\frac{\partial T}{\partial t} + \boldsymbol{u} \cdot \nabla T = \nabla \cdot (\alpha \nabla T) + \Psi, \qquad (2.3)$$

where T is the temperature, Ψ is a source term (set to zero here) and α is the thermal diffusivity. Equation (2.3) can be solved in the framework of LBM where (2.1) and (2.2) are used with τ replaced by τ_T (time relaxation for the temperature) and $f_i(\boldsymbol{x}, t)$ is replaced by $f_i^T(\boldsymbol{x}, t)$, the temperature density distribution. The temperature at a computational node is calculated as $T = \sum_i f_i^T$. The temperature relaxation time τ_T

is related to τ through the Prandtl number,

$$Pr = \frac{\nu}{\alpha} = \frac{2\tau - 1}{2\tau_T - 1}, \tag{2.4}$$

where ν is the kinematic viscosity of the fluid.

2.3. *Computational domain and boundary conditions*

The three-dimensional computational domain, which includes the square cylinder, is Cartesian and has $800 \times 110 \times 110$ mesh points (or $80d \times 11d \times 11d$, d is the *diameter* of the square cylinder represented with 10 mesh points). The mesh increments in the three directions are equal ($\Delta x = \Delta y = \Delta z = \Delta = 0.1d = 1$). The cylinder is placed at a distance of $9d$ after the inlet where a constant velocity U_0 is imposed. Periodic conditions are applied on the lateral sides of the computational domain and a convective boundary condition is imposed at the outlet. A no-slip condition is applied on the cylinder surface. This condition is easily implemented in LBM through the so-called bounceback scheme (Succi 2001). The surface of the cylinder is kept at a constant temperature $T_w = 3$ (lattice unit), and the incoming fluid is at a temperature $T_0 = 1$. The Reynolds number $R_d (= U_0 d/\nu)$ is 200 and the Prandtl number is 0.7.

The number of mesh points used to represent the cylinder diameter is selected for allowing computations to be done over a relatively long distance behind the cylinder. The number is sufficient to capture the features of the transitional flow accurately. For example, the computed Strouhal number ($St = fd/U_0$, f is the shedding frequency) was about 0.127, a value close to those obtained in several experimental and numerical studies (see for examples Durão, Heitor & Pereira 1988; Liou, Chen & Hwang 2002; Shadaram, Fard & Rostamy 2008).

The computations were carried out on a cluster of 8 dual processors where the MPI2 protocol was used to perform the parallelization.

3. Results

3.1. *Validation of the LBM simulation*

Although it is not the scope of the present paper, it is should be mentioned that the results of the LBM simulation of the three-dimensional natural transition in a cylinder wake were compared against existing data (Djenidi & Antonia 2008). We briefly summarize the comparison here. The simulation predicted the early stages of the transition to turbulence quite accurately. In particular, modes A and B were captured reliably and were in agreement with published data (Williamson 1996*a*, *b*). After the first instability leading to the von Kármán mode when spanwise vortices were shed from the cylinder, a transient period developed. During this period and while the flow remained two-dimensional, a very small spanwise velocity component w developed gradually and became organized into distinct 'cells'. This velocity component resulted from the development of weak longitudinal counter-rotating vortices along the cylinder. These results were in a very good agreement with the DNS of Persillon & Braza (1998) and Braza (1999). The flow pattern at the present Reynolds number (figure 1, Ω is the instantaneous vorticity magnitude) is consistent with previous studies of transitional flow in a circular cylinder wake (Williamson 1996*a*): rows of spanwise vortices linked by 'braids' of vorticity. The spanwise spacing λ_z between the braid structures were about $1d$ indicating that the flow was in the early stages of mode B of the transition regime at this Reynolds number (Williamson 1996*b*).

FIGURE 1. Isocontour of the instantaneous vorticity, $\Omega/\Omega_{max} = 0.1$.

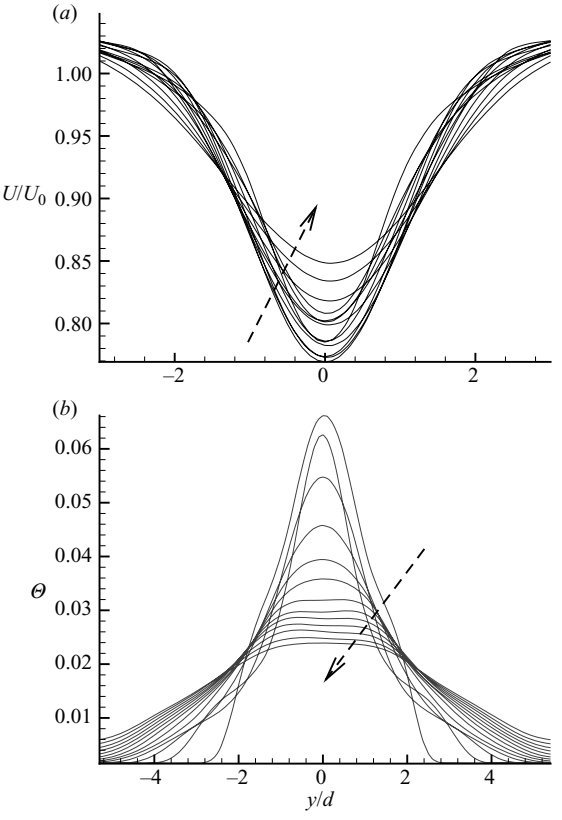

FIGURE 2. Profiles of the longitudinal mean velocity and mean temperature at regular intervals between $x/d = 5$ and 65. The arrow indicates the increasing x.

3.2. *Mean velocity and temperature fields*

Profiles of the longitudinal mean velocity U and mean temperature Θ at several positions downstream of the cylinder are reported in figure 2 (here and hereafter the data are normalized by U_0, $\Delta T_0 = T_w - T_0$ and d). The mean quantities have been obtained by averaging the instantaneous data over both time and z direction using 120 independent fields. Both U and Θ are symmetric with respect to $y/d = 0$. While the mean velocity profiles are consistent with those obtained by Paranthoën *et al.* (2004) and Godard *et al.* (2005), the mean temperature profiles differ significantly. These authors showed that Θ presented a symmetrical double peaked distributions when

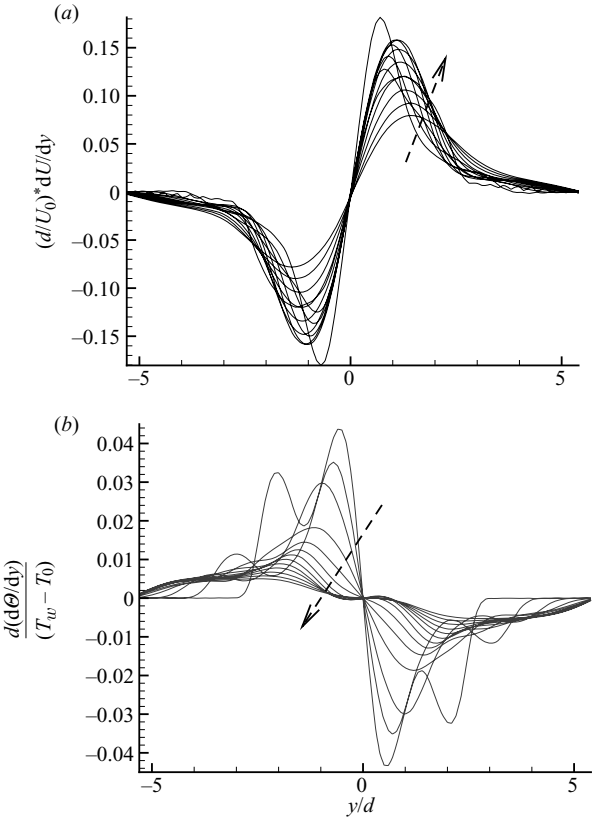

FIGURE 3. Profiles of the mean velocity gradient $\mathrm{d}U/\mathrm{d}y$ and mean temperature gradient $\mathrm{d}\Theta/\mathrm{d}y$ at regular intervals between $x/d = 5$ and 65. The arrow indicates the increasing x.

the heat line source was located at $y/d = 0$. When they had the line source off axis, a single peaked profile was obtained with the peak located off axis. It should be stated that the present simulations also showed a double peaked distribution when $x/d < 1$ (not shown here). One would expected that for large x/d the mean temperature profile from a line source will eventually become a single peaked distribution with the peak at $y/d = 0$. This is in fact the trend the data of Paranthoën *et al.* (2004) indicated. The difference in the mean temperature profile between the present results and that of Paranthoën *et al.* (2004) and Godard *et al.* (2005) highlights the influence of the heat source geometry on the transport of heat in the near-wake region.

Although not well discernible in figure 2, the temperature profile does not decay monotonically. This is better seen in figure 3 showing profiles of $\mathrm{d}U/\mathrm{d}y$ and $\mathrm{d}\Theta/\mathrm{d}y$ (d./dy represents the partial derivative with respect to y). While $\mathrm{d}U/\mathrm{d}y$ decays monotonically with increasing x, $\mathrm{d}\Theta/\mathrm{d}y$ presents strong variations. For example, the peak nearer to $y/d = 0$ decreases before increasing again. Only for $x/d > 25$ is the decay of $\mathrm{d}\Theta/\mathrm{d}y$ monotonic. This certainly shows that the vorticity has a strong impact on the temperature field in the near-wake region where the vortical structures are found to be well defined. This impact is clearly seen in figures 4 and 5 which show isocontours of the magnitude of the instantaneous vorticity Ω and temperature T. Notice the quasi-perfect correspondance between the contours of Ω and T, particularly in the region $0 \leqslant x/d \leqslant 30$. It is as if the thermal structures ride on

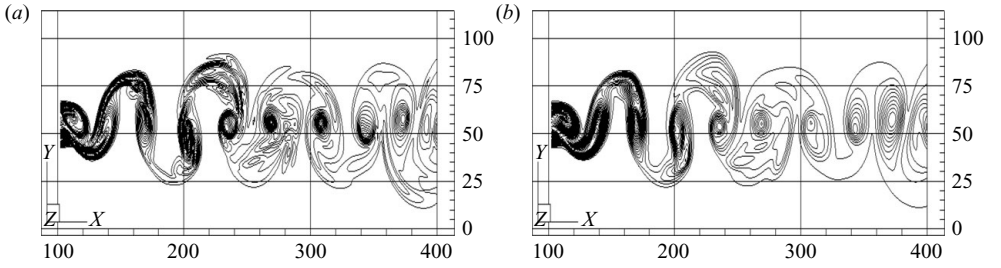

FIGURE 4. Isocontours of the magnitude the instantaneous vorticity (*a*) and temperature (*b*) in the x–y plane at $z/d = 0$ for $0 \leqslant x/d \leqslant 30$.

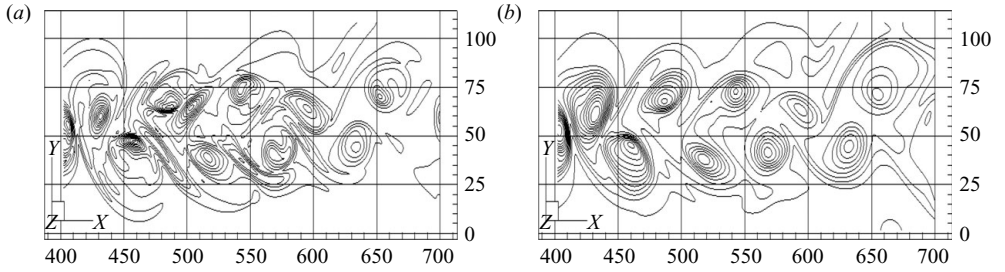

FIGURE 5. Isocontours of the magnitude of the instantaneous vorticity (*a*) and temperature (*b*) in the x–y plane at $z/d = 0$ for $30 \leqslant x/d \leqslant 60$.

the back of the vortical structures. Mi & Antonia (1993) and Matsumura & Antonia (1993) reported a similar correspondance between T and the spanwise component of the vorticity Ω_z in their turbulent heated cylinder wake at a Reynolds number of about 5400 and 5900, respectively. These results along with the present ones are reminiscent of the results of Mi & Antonia (1994) and confirm that heat can be an effective passive marker of vortical structures, at least as long as these structures are well defined.

3.3. *Momentum and heat transport*

The velocity and temperature fluctuations have been calculated and their statistics computed. The distributions of the r.m.s. of the three velocity fluctuation components, u', v' and w', are shown in figure 6 (the prime denotes the r.m.s.). A number of observations can be made. As expected the profiles are reasonably symmetrical with respect to $y/d = 0$. The scatter found on some of the u' and w' profiles reflects the number of fields used for averaging the data. The component v' is larger than u' which is larger than w', illustrating the strong global anisotropy of the flow, although this anisotropy decreases as x/d increases. While the v' distributions present a single peak at $y/d = 0$, u' evolves from a double peak to a single peak distribution. The local maxima of u' occur at the y/d positions where the magnitude of $\mathrm{d}U/\mathrm{d}y$ is maximum. Interestingly, the w' component shows also a double peak distribution in the region up to x/d of about 7; a double peak is clearly seen in the distribution at $x/d = 5$ but is less evident at higher downstream distances. The double peak in the w' distributions is also observed at higher Reynolds numbers. The higher values of v' over the other two components are related to the alternative feature of the vortex shedding. More kinetic energy is transferred into the lateral velocity component than into the longitudinal and spanwise ones. This is observed in the data of Paranthoën

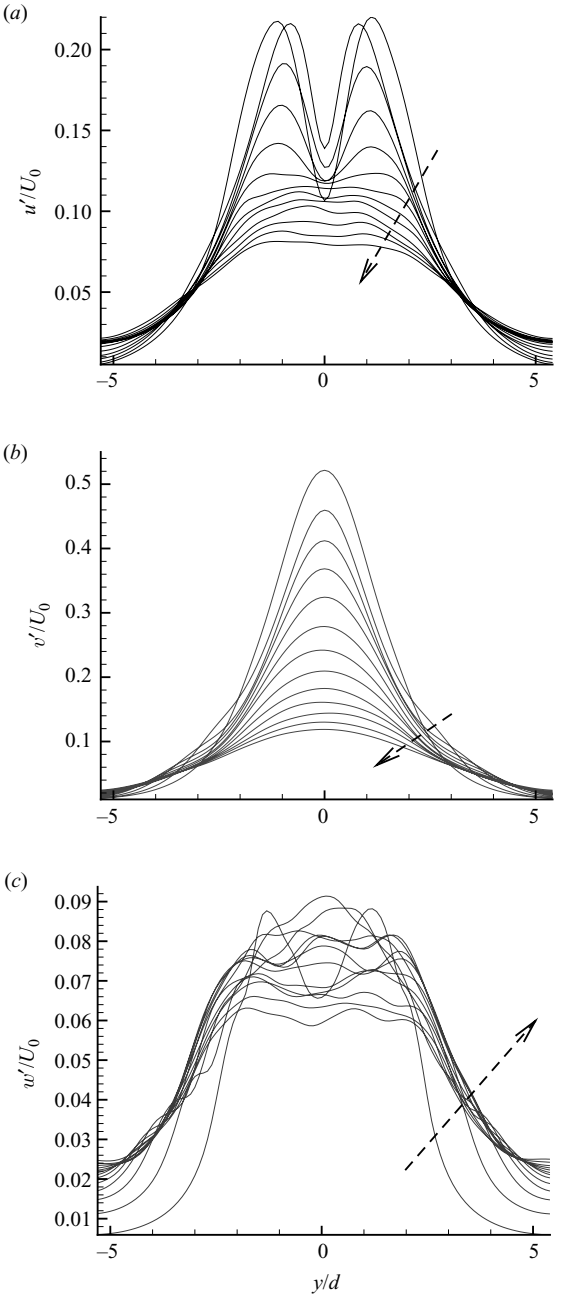

FIGURE 6. Profiles of the r.m.s. (*a*) longitudinal u', (*b*) transverse v' and (*c*) spanwise w' velocity fluctuations at regular intervals between $x/d = 5$ and 65. The arrow indicates the increasing x.

et al. (2004) and Godard *et al.* (2005). In cylinder wakes at much higher Reynolds numbers u' becomes the dominant component after a relatively shorter downstream distance than the present case.

The r.m.s. of the temperature fluctuations θ' is symmetrical with respect to $y/d = 0$, but its evolution is not monotonic (figure 7). The distribution is single peaked for

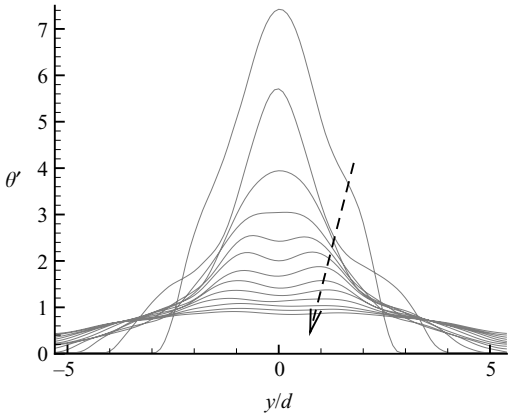

FIGURE 7. Profiles the r.m.s. temperature fluctuations θ' at regular intervals between $x/d = 5$ and 65. The arrow indicates the increasing x.

$0 < x/d < 20$ then becomes double peaked for $x/d > 25$. Godard *et al.* (2005) also observed this evolution. It seems that for $x/d > 68$ the distribution tends to return towards a single peaked profile. At high Reynolds numbers the distributions of passive scalars become more rapidly single peaked (Rehab *et al.* 2000). Notice that the humps observed in the distributions at $y/d = \pm 2$ for $x/d = 15$ and $y/d = \pm 3$ for $x/d = 20$ correspond to local peaks in the $\mathrm{d}\Theta/\mathrm{d}y$ profiles (figure 3). These humps, also visible in the mean temperature profile (see figure 2), mark the influence of the von Kármán vortex street on the temperature field in the early stage of the wake as demonstrated in figures 4 and 5.

The alternative character of the shedding in the flow is also reflected in the distributions of the Reynolds shear stress $\overline{uv}$ and the heat fluxes $\overline{u\theta}$ and $\overline{v\theta}$ shown in figures 8 and 9 (the overbar denotes an average with respect to time and the z direction). The profiles of $\overline{uv}$ and $\overline{v\theta}$ are antisymmetrical with respect to $y/d = 0$, while $\overline{u\theta}$ is symmetrical. However, the distributions present strong variations within the region x/d up to about 30, illustrating the complex features of the flow structure in this region, where rows of spanwise vortices are linked by braids of vorticity (see figure 1). For x/d higher than about 50, where the flow is dominated by less coherent structures, the profiles are similar to those observed at high Reynolds numbers. While the distributions of $\overline{uv}$ and $\overline{v\theta}$ are consistent with those observed in Godard *et al.* (2005), $\overline{u\theta}$ is markedly different. In the latter study, $\overline{u\theta}$ is negative at practically all downstream locations of the wake. This contrasts with the present results which show positive values of $\overline{u\theta}$ on both sides of the centreline. The magnitude of the positive peaks reduces as x/d increases; at $x/d = 65$, $\overline{u\theta}$ becomes negative at all y/d. Matsumura & Antonia (1993) results show that the distributions of $\overline{u\theta}$ for $x/d < 10$ present similar features to the distributions in figures 8 and 9; at $x/d > 20$, $\overline{u\theta}$ was negative at all y/d. They attributed the positive values of $\overline{u\theta}$ to the coherent motion associated with the vortical structures. The decrease of the magnitude of the peaks in $\overline{u\theta}$, as x/d increases, concords with the decay of the coherent structures.

The magnitude of $\overline{u\theta}$ is larger than that of $\overline{v\theta}$ in the region $5 < x/d < 45$. This differs from the data of Matsumura & Antonia (1993) and Godard *et al.* (2005) which showed that $\overline{v\theta}$ is always larger than $\overline{u\theta}$. While at present no definitive explanation is given, one may argue that both the rolls of spanwise vortices and the vorticity braids would contribute more to $\overline{u\theta}$ than $\overline{v\theta}$. In the experiment of Godard *et al.* (2005) the cylinder

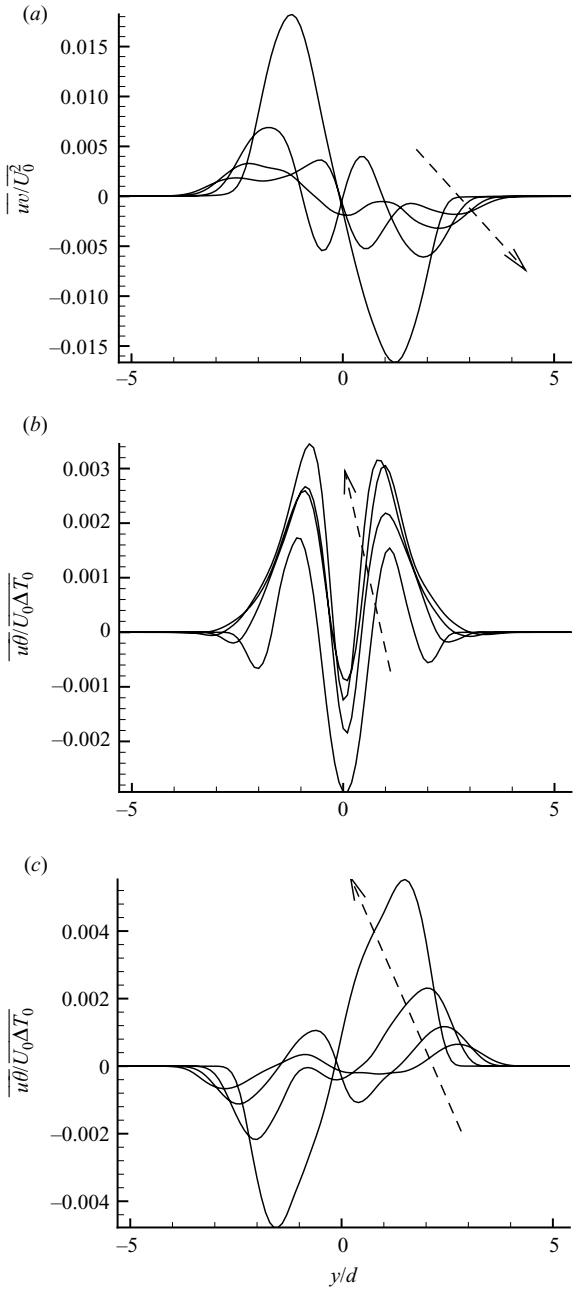

FIGURE 8. Profiles of the shear stress $\overline{uv}$ (*a*) and the heat fluxes $\overline{u\theta}$ and $\overline{v\theta}$ (*b*, *c*) at regular intervals between $x/d = 5$ and 11. The arrow indicates the increasing x.

wake was two-dimensional with the von Kármán vortices well defined and no vorticity braids. In the study of Matsumura & Antonia (1993), where the Reynolds number was much higher than here ($R_d = 5900$), the three-dimensional-transitional region was short, which might explain why $\overline{u\theta}$ was already smaller than $\overline{v\theta}$ at $x/d = 10$. It would be worthwhile to carry out measurements in the same conditions as those of the latter

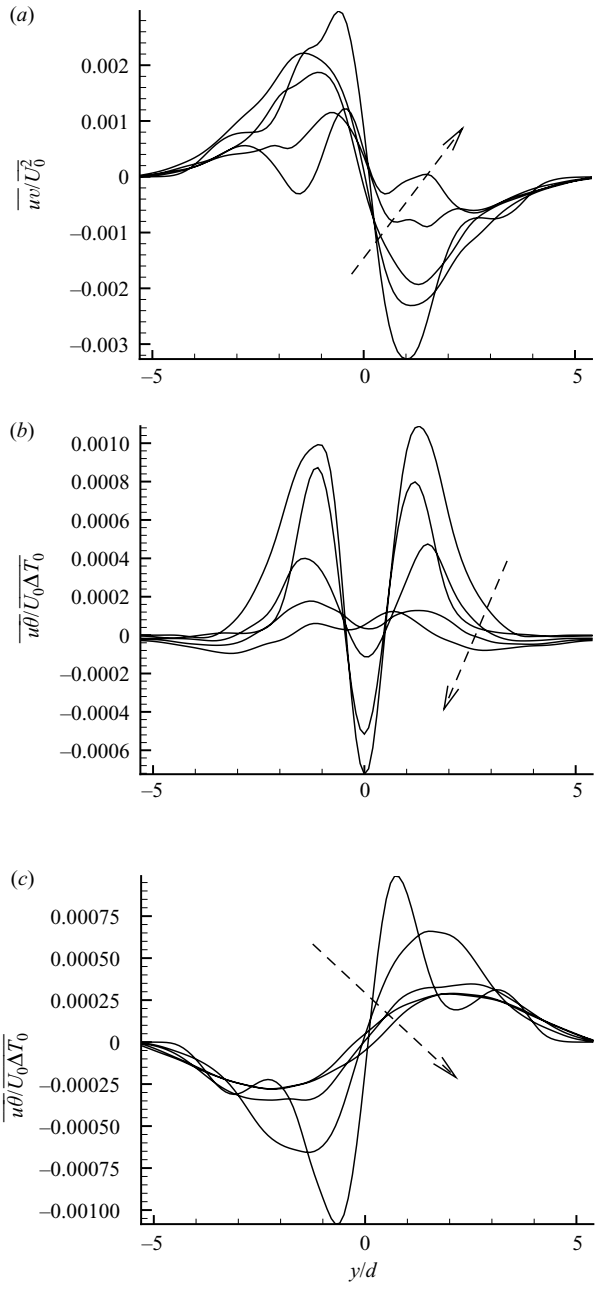

FIGURE 9. Profiles of the shear stress $\overline{uv}$ (*a*) and the heat fluxes $\overline{u\theta}$ and $\overline{v\theta}$ (*b*, *c*) at regular intervals between $x/d = 15$ and 65. The arrow indicates the increasing x.

authors but at closer downstream distances from the cylinder to determine whether or not $\overline{u\theta}$ is larger than $\overline{v\theta}$.

The profiles of $\overline{uv}$ and $\overline{v\theta}$ show a degree of symmetry to each other, although less pronounced for $x/d > 20$. Similar observations can be made in the heated cylinder wake studies quoted above. This may imply that $\overline{uv}$ and $\overline{v\theta}$ are approximately proportional to each other, which would be of interest from a heat transfer modelling

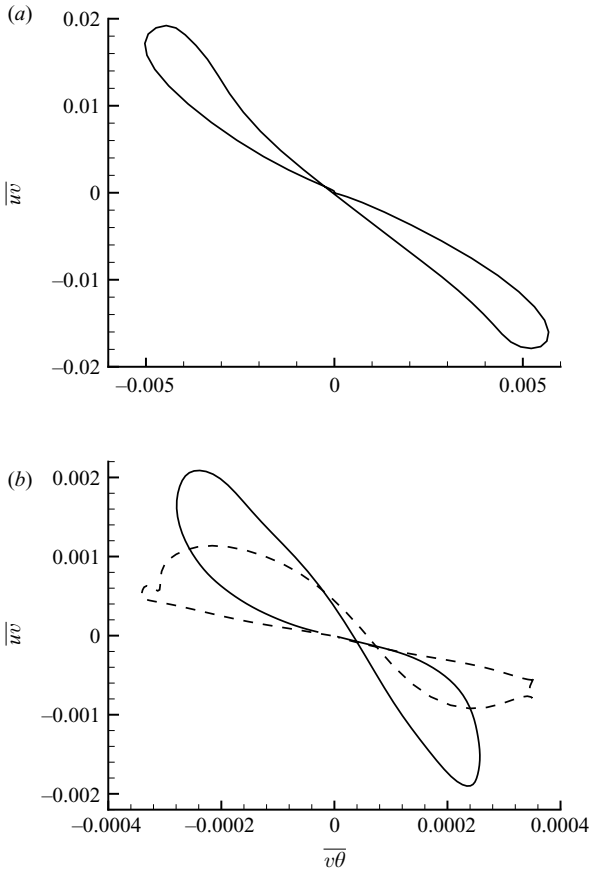

FIGURE 10. Profiles of $\overline{uv}$ versus $\overline{v\theta}$. (*a*) $x/d = 5$ (*b*) $x/d = 35$ (dashed line) and 65 (solid line).

point of view. Figure 10, which shows plots of $\overline{uv}$ as function of $\overline{v\theta}$ for $x/d = 5d$, $35d$ and $65d$, indicates that while this is not quite exact (a perfect proportionality between $\overline{uv}$ and $\overline{v\theta}$ would be indicated by a straight line passing through (0, 0)), one may, as a first-order approximation, assume that $\overline{uv} = C_\theta \overline{v\theta}$ with the constant C_θ equal to the slope of a straight line representing the principal axis of the closed curve $C(\overline{uv}, \overline{v\theta})$. Note that, since the slope of this axis changes with x/d, C_θ would have to be a function of x/d.

Overall, $\overline{uv}$ and $\overline{v\theta}$ are of opposite sign to $\mathrm{d}U/\mathrm{d}y$ and $\mathrm{d}\Theta/\mathrm{d}y$, respectively, across the wake. For some x/d locations though (e.g. 9 and 11) this is not true. At these positions, $\overline{uv}$ has the same sign as $\mathrm{d}U/\mathrm{d}y$ in the central region of the wake. Similar observations can be made for $\overline{v\theta}$ and $\mathrm{d}\Theta/\mathrm{d}y$. Also at $x/d = 25$, one can see that $\mathrm{sign}(\overline{uv}) = \mathrm{sign}(\mathrm{d}U/\mathrm{d}y)$ in the region $1 \leqslant |y/d| \leqslant 3$. The fact that $\mathrm{sign}(\overline{uv}) = -\mathrm{sign}(\mathrm{d}U/\mathrm{d}y)$ and $\mathrm{sign}(\overline{v\theta}) = -\mathrm{sign}(\mathrm{d}\Theta/\mathrm{d}y)$ in most part of the wake is consistent with a GTM for $\overline{uv}$ and $\overline{v\theta}$. However, this is only approximately confirmed by the data as seen in figures 11 and 12, where $\overline{uv}$ and $\overline{v\theta}$ at the downstream locations of $x/d = 5, 35$ and 65 are plotted as functions of $\mathrm{d}U/\mathrm{d}y$ and $\mathrm{d}\Theta/\mathrm{d}y$, respectively. In these representations, quadrants 1 and 3 correspond to GTMs, $\overline{uv} = -\nu_t \times (\mathrm{d}U/\mathrm{d}y)$ and $\overline{v\theta} = -\nu_{t,\alpha} \times (\mathrm{d}\Theta/\mathrm{d}y)$, where ν_t and $\nu_{t,\alpha}$ are the turbulent viscosity and turbulent thermal diffusivities. GTMs would be observed across the wake if the data collapsed

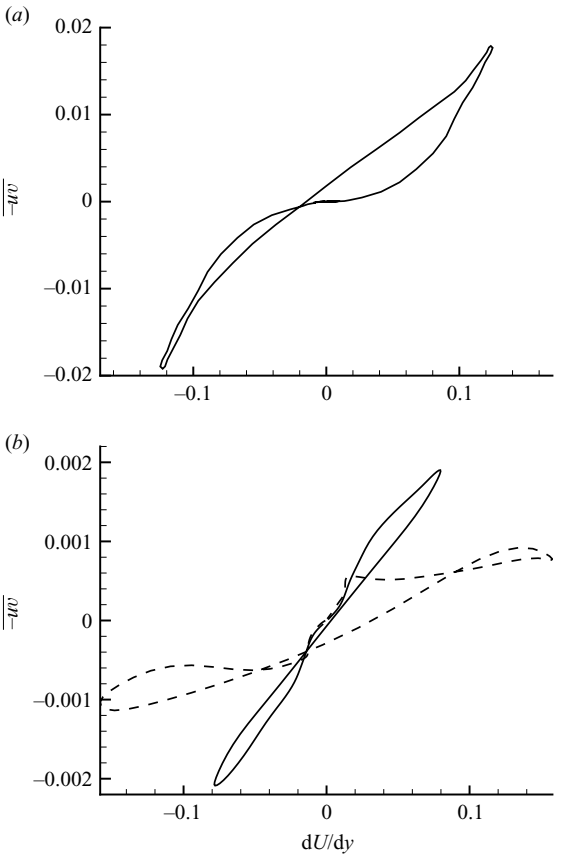

FIGURE 11. Profiles of $-\overline{uv}$ versus dU/dy. (*a*) $x/d = 5$ (*b*) $x/d = 35$ (dashed line) and 65 (solid line).

into single curves; constant ν_t and $\nu_{t,\alpha}$ would be indicated by straight lines passing through the point (0, 0). Notice that the magnitudes of $\overline{uv}$ and $\overline{v\theta}$ are reduced by a factor 10 between the positions $x/d = 5$ and 35, which is why the data for $x/d = 5$ have been plotted separately. The shape of the curves (inclined 8-shaped) formed by the data unambiguously demonstrates that neither $\overline{uv}$ nor $\overline{v\theta}$ can be strictly modelled by a GTM throughout the entire wake. Yet, it would be relatively appropriate to argue that the data tend to gather around straight lines passing through the point (0, 0). The rather thin elongated shape of the curves in figure 11 suggests that a GTM may, to a first-order approximation, be used to model $\overline{uv}$. In particular, one section of the curve at $x/d = 65$ does present a straight line in the region corresponding to $-0.08 < \mathrm{d}U/\mathrm{d}y < 0.08$. The region of the wake to which this straight line section corresponds is the central part of the wake ($-2 \leqslant y/d \leqslant 2$), implying that a GTM is valid in this region. While data of figure 12 may allow a GTM to be used to model $\overline{v\theta}$ for $x/d = 65$, it would certainly be less accurate than that for $\overline{uv}$, as the 8-shaped curves are less elongated than those of figure 11. Whether the curves in these figures would approach a straight line, at least in the central part of the wake, for x/d extending beyond 65 remains to be determined. One needs to extent the present simulations to include the far wake region in order to provide a conclusive statement. Quite interestingly, some parts of the curves in both figures are located

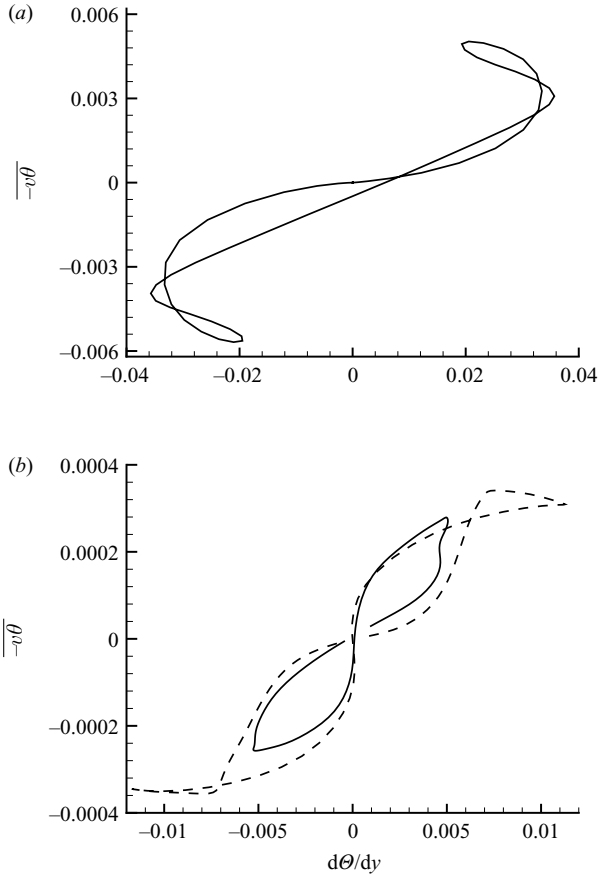

FIGURE 12. Profiles of $-\overline{v\theta}$ versus $d\Theta/dy$. (*a*) $x/d = 5$ (*b*) $x/d = 35$ (dashed line) and 65 (solid line).

in the second (figure 11, $x/d = 5$) and fourth (figure 11, $x/d = 35$; figure 12, $x/d = 5$) quadrants, which corroborates the earlier observations on the signs of $\overline{uv}$, $\overline{v\theta}$, dU/dy and $d\Theta/dy$. Paranthoën *et al.* (2004) and Godard *et al.* (2005) also found that some of their data $\overline{v\theta}$ were located in the second and fourth quadrants. The 'excursions' of data in these quadrants reveal that counter-gradients occur only in localized regions of the present flow. While the cause of the occurences of these counter-gradients is not known yet, one may argue that they may be related to the orientation and/or locations of the intantaneous vortices within the wake. Indeed, it can be seen in figures 4 and 5 that the spatial arrangment of the (spanwise) vortices changes significantly in the region $x/d \leqslant 40$, where counter-gradients are observed in this region of the wake. The vortices are initially aligned with the centreline of the wake before moving radially away from it as x/d increases beyond 35. A Similar argument can be made for the sign of $\overline{v\theta}$, although no counter-gradient is observed for $x/d \geqslant 30$.

The seemingly resemblance between figures 11 and 12 could suggest a possible analogy between the momentum and heat transports. To assess this possibility, the turbulent Prandtl number, $Pr_t = \nu_t/\nu_{t,\alpha}$, was calculated and is shown in figure 13 for $x/d = 5, 35$ and 65. No data smoothing has been done; notice the discontinuity at $y/d = 0$ due to the zero gradients there. A constant Pr_t with a value of 1

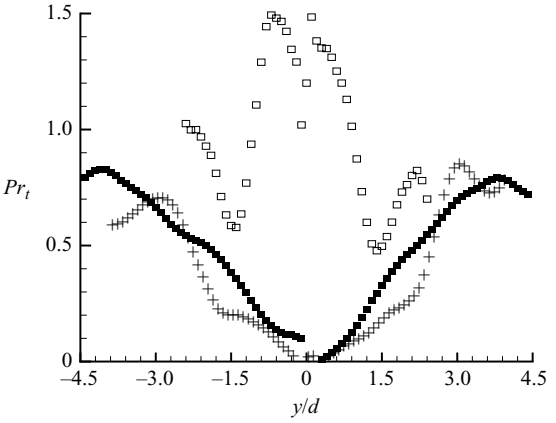

FIGURE 13. Profiles of the turbulent Prandtl number, Pr_t at $x/d = 5$ (open squares), 35 (crosses) and 65 (solid squares).

would indicate a Reynolds analogy between $\overline{uv}$ and $\overline{v\theta}$ across the wake. Clearly, no such result is observed. Not only Pr_t is not equal to one, but its behaviour differs significantly between the position $x/d = 5$ and the other two, highlighting variations in the momentum and heat transports between the near-wake and the intermediate wake regions. In general, the momentum appears to be more effectively transported in the very near-field region of the wake, which is indicated by the relatively high values of Pr_t at $x/d = 5$. As the downstream distance increases behind the cylinder, heat becomes more effectively transported than momentum as reflected in the small values of Pr_t for $x/d = 35$ and 65. Furthermore, at these distances the transport of heat is more effective in the central region of the wake than in the outer regions, although the data indicate that the effectiveness decreases as the distance x/d increases. There appears to be a region of about $25d$ to $35d$ where heat is most effectively transported. Godard *et al.* (2005) also noted that heat was more efficiently transported than momentum. Antonia, Zhou & Matsumura (1993) found that Pr_t was about 1 at $x/d = 10$, but substantially less than one in the central region of the wake for $x/d > 20$.

3.4. *Topology of the fluctuating velocity and temperature fields*

Figures 14 shows examples of isocontours of the three components of the fluctuating velocity and the temperature fluctuation in the region $0 \leqslant x/d \leqslant 30$. Clearly, all fluctuating components are organized into well-defined coherent structures of relatively large scales, with similarities between them. The u and v structures are both organized into transverse rolls, while w is formed into mainly braid-like structures and a few discontinuous rolls. The θ structures present a mixture of rolls and braids. Notice though that the θ field bears more similarity with w than u and v. This is confirmed in figures 15 and 16 which shows instantaneous isocontours of the velocity and temperature fluctuations in the x–y plane at $z/d = 0$. Despite the difference in the spatial organization, the contours of θ present a relatively good level of correspondance with the w contours throughout the wake. Interestingly, while the correspondance of contours between u and v is weak, that between v and w and, consequently, θ is better at large x (figure 16) than closer to the cylinder (figure 15). Note though the non-staggered arrangement of the v structures as compared to the others.

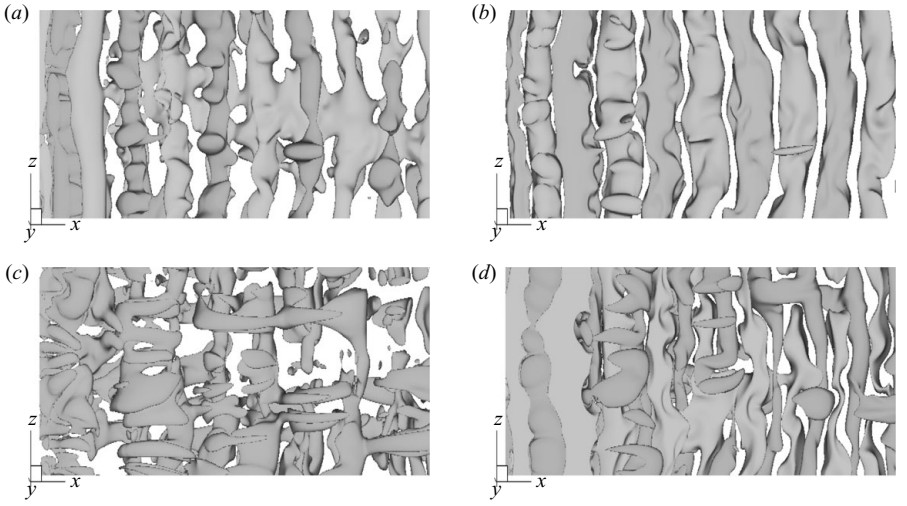

FIGURE 14. Instantaneous isocontours of $u/U_0 = \pm 0.15$ (a), $v/U_0 = \pm 0.25$ (b), $w/U_0 = \pm 0.08$ (c) and $\theta/(T_w - T_0) = \pm 0.02$ (d) in the region $0 \leqslant x/d \leqslant 30$.

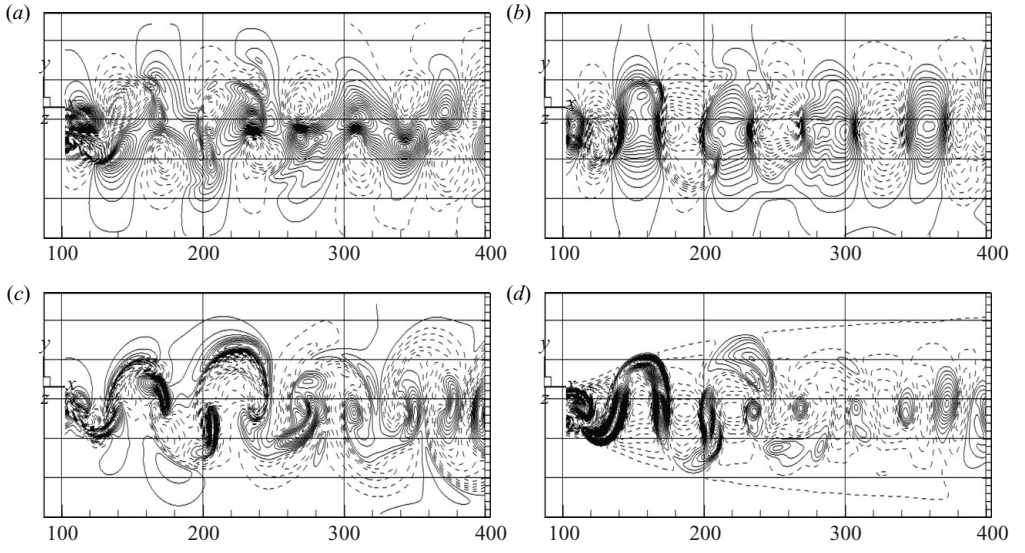

FIGURE 15. Instantaneous isocontours of u (a), v (b), w (c) and θ (d) in the x–y plane at $z/d = 0$ and in the region $0 \leqslant x/d \leqslant 30$. Solid lines: positive contours, dashed lines: negative contours.

The fluctuating velocity structures reflect the contributions of the fluctuating vorticity components, ω_x, ω_y and ω_z, to the velocity field (figure 17). For example, comparing figures 14 and 17 clearly shows that both ω_x and ω_y, which are organized into braids, are the main contributors to the spanwise fluctuating velocity. Likewise, the very strong contribution of ω_z to both u and v is observed in the fact that these three components are organized into similar structures. It was found that ω_z was larger than ω_x which in turn was bigger than ω_y. This then explains why v is larger than u and w (see figure 6): it receives contributions from ω_z and ω_x, the two largest

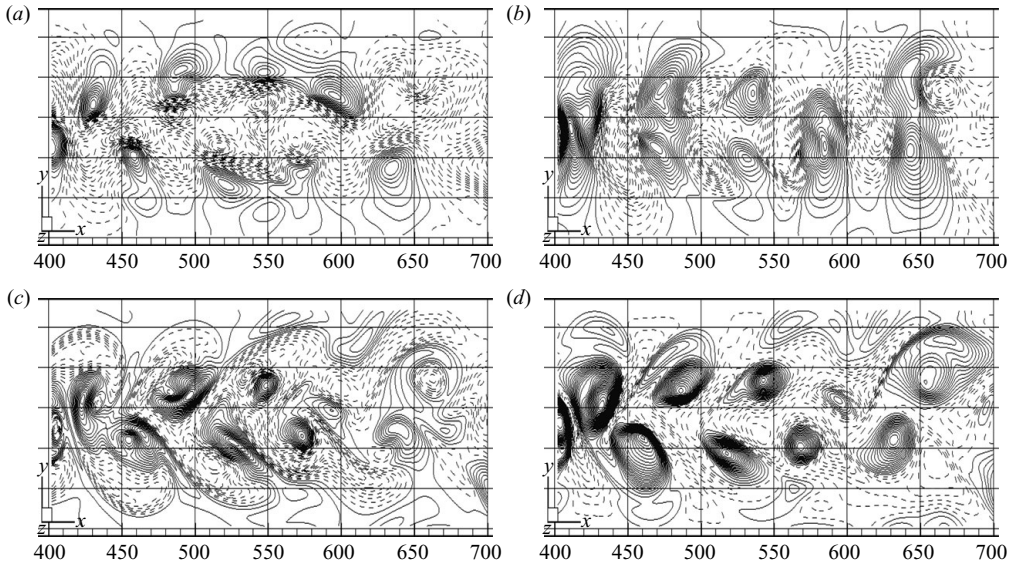

FIGURE 16. Instantaneous isocontours of u (a), v (b), w (c) and θ (d) in the x–y plane at $z/d = 0$ and in the region $30 \leqslant x/d \leqslant 60$. Solid lines: positive contours, dashed lines: negative contours.

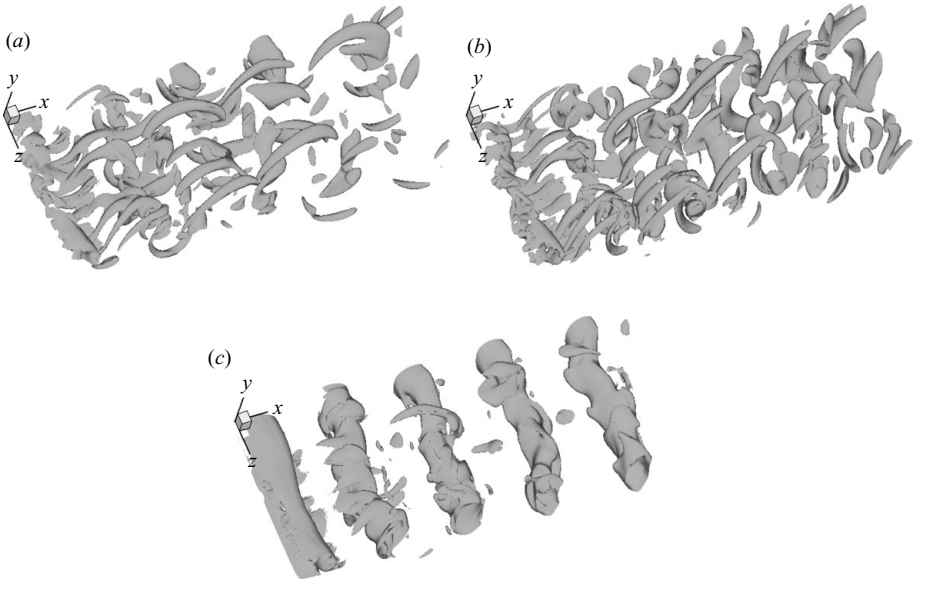

FIGURE 17. Instantaneous isocontours of $\omega_x/\omega_{x,max} = -0.05$ (a), $\omega_y/\omega_{y,max} = -0.05$ (b) and $\omega_z/\omega_{z,max} = -0.05$ (c) in the region $0 \leqslant x/d \leqslant 30$.

fluctuating vorticity components. The component u which is larger than w, receives contributions from ω_z and ω_y.

After the initial stage of the shedding, the velocity and thermal structures tend to align along the wake centreline in the region $10 \leqslant x \leqslant 35$ before moving away from it in the region $x \geqslant 40$. This is particularly evident for v and θ. This indicates that the fluctuating velocity field affects quite strongly the fluctuating temperature field,

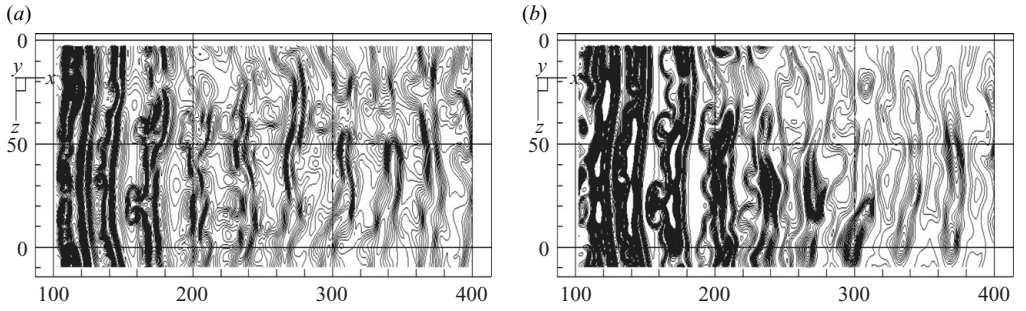

FIGURE 18. Instantaneous isocontours of q^2 (a) and θ^2 (b) at $y/d = 0$ in the region $0 \leqslant x/d \leqslant 30$.

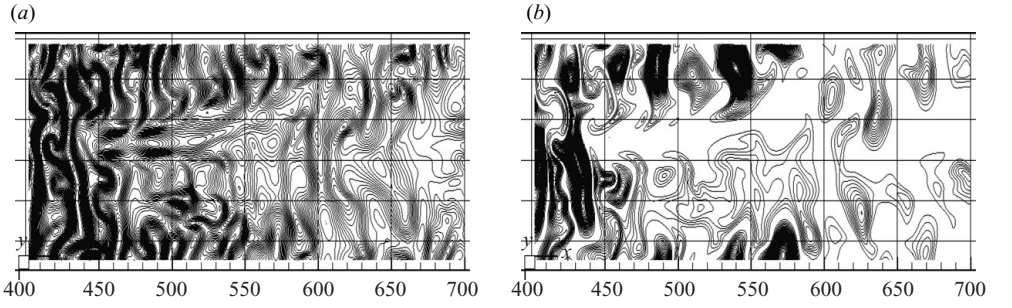

FIGURE 19. Instantaneous isocontours of q^2 (a) and θ^2 (b) at $y/d = 0$ in the region $30 \leqslant x/d \leqslant 60$.

which in turn would imply that the sum of u, v and w could bear some analogy with θ. To assess this point, contours of the fluctuating turbulent kinetic energy, $q^2(=0.5(u^2+v^2+w^2))$, and θ^2 in the x–z plane at $y/d = 0$ are presented in figures 18 and 19. There is a remarkably good correspondence between the isocontours of θ^2 and q^2 throughout the entire wake. It should be reported, though, that the thermal structures present sharper edges than the q^2 structures (this is well seen in a xy view, not shown here). Antonia, Abe & Kawamura (2009) also reported very good similarity between θ^2, q^2 and u^2 isocontours in the near-wall region of a turbulent channel flow with one heated wall. Their data also show sharper edges for θ^2 than u^2. These authors argue that this feature is likely to reflect the fact that the scalar is less mixed than u.

A final and quite interesting point to note and comment on is the locations of θ_{max}, the maxima of θ in figures 15 and 16. These locations correspond to the locations of very strong velocity gradients. This is very well seen in figure 20 where the positive θ_{max} have been superposed onto the isocontours of the velocity components in the region $30 \leqslant x/d \leqslant 60$ (similar evidence is observed in the region $0 \leqslant x/d \leqslant 30$). The maxima appear to be located where the fluctuating velocity contours are most compressed, that is at locations of high velocity gradients (a similar correspondence with the w contours, not shown here, is also observed). Notice the almost perfect correspondence between the positive θ_{max} locations and the interfaces between positive and negative v isocontours. These results suggest a possible relation between the temperature fluctuation gradients, $\partial\theta/\partial x_i$, and ω_{x_i} or at least $\partial u_i/\partial x_i$. This would be consistent with the observation made in a heated turbulent channel flow (Abe,

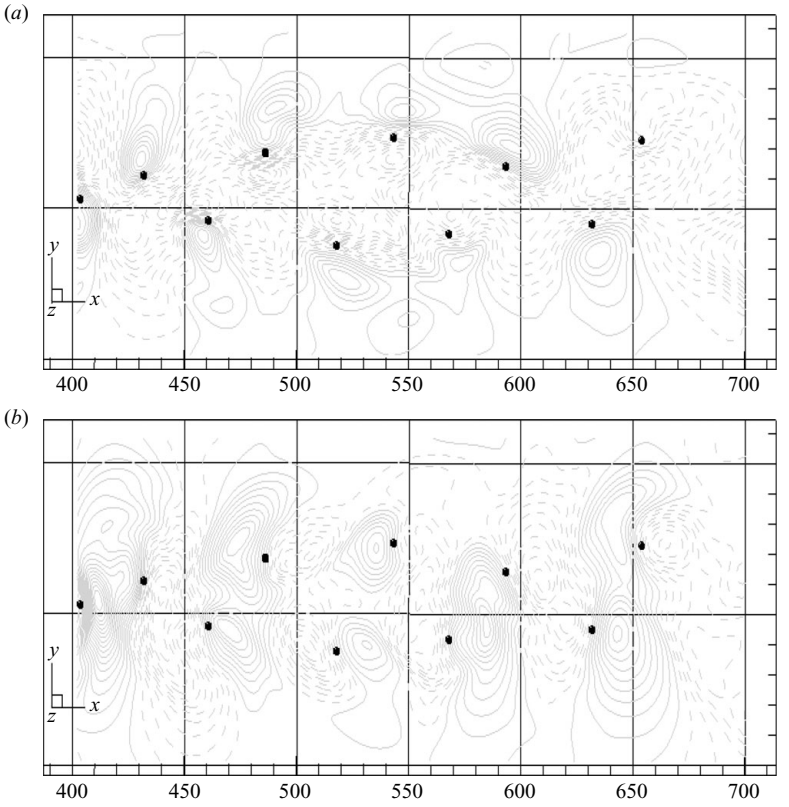

FIGURE 20. Instantaneous isocontours of u (a), v (b), with superposed local maxima of positive θ (black points) in the x–y plane at $z/d = 0$ and in the region $30 \leqslant x/d \leqslant 60$.

Antonia & Kawamura 2009) that $\partial\theta/\partial x_i$ are interlinked with ω_{x_i}. Also of relevance to the present results is that Godard (2001) observed that $\partial\theta/\partial x_i$ tends to be aligned with the principal compressive (negative) strain rate directions.

4. Conclusions

The momentum and heat transport of a three-dimensional transitional wake of a heated square cylinder has been investigated using DNS based on the LBM. The simulations were run for a Reynolds number of about 200 and a Prandtl number of 0.7. The spatial resolution was considered adequate for capturing the salient features of the transitional flow relevant to the transport of momentum and heat.

It was found that while momentum and heat were transported by vortical structures, heat was more effectively transported than momentum, except close to the cylinder ($5 \leqslant x/d$) where the reverse occurred. This explained why the Reynolds analogy between $\overline{uv}$ and $\overline{v\theta}$ was not observed in this flow. Furthermore, the heat flux $\overline{u\theta}$ was larger than $\overline{v\theta}$ in the region $5 \leqslant x/d \leqslant 45$. This unexpected feature was thought to be associated with the structural nature of the transitional flow. A possible explanation is that the strongly coherent vortical structures (roll and braids) particular to this flow in this region of the wake contribute more to $\overline{u\theta}$ than $\overline{v\theta}$.

Although $\overline{uv}$ and $\overline{v\theta}$ were respectively of opposite sign to $\mathrm{d}U/\mathrm{d}y$ and $\mathrm{d}\Theta/\mathrm{d}y$ which is consistent with a GTM, the data analysis showed that the GTM can only be a first

order approximation, the approximation being better for $\overline{uv}$ than $\overline{v\theta}$. It should be pointed out though that counter-gradients were observed in localized regions, which excludes any possible use of GTM in these regions.

The analysis of the topology of the fluctuating fields showed that the fluctuating temperature field presented thermal structures similar to the velocity structures with, however, a different spatial organization. Futhermore, a relatively good correlation between the q^2 and θ^2 fields was observed, implying an analogy between these two quantities.

Finally, the data showed that the local maxima of θ coincided with the maxima of fluctuating velocity gradients, hinting to a possible relationship between temperature gradients and vorticity and/or velocity gradients. This issue needs further investigation.

REFERENCES

Abe, H., Antonia, R. A. & Kawamura, H. 2009 Correlation between small-scale velocity and scalar fluctuations in a turbulent channel flow. *J. Fluid Mech.* **627**, 1–32.

Antonia, R. A., Abe, H. & Kawamura, H. 2009 Analogy between velocity and scalar fields in a turbulent channel flow. *J.* Fluid Mech. **628**, 241–268.

Antonia, R. A., Chambers, A. J., Britz, D. & Browne, L. W. B. 1986 Organized structures in a turbulent plane jet: topology and contribution to momentum and heat transport. *J. Fluid Mech.* **172**, 211–229.

Antonia, R. A. & Mi, J. 1993 Vorticity and temperature distributions for an isolated viscous vortex. *Tech. Rep.* T.N. -FM 93/02. University of Newcastle.

Antonia, R. A., Zhou, Y. & Matsumura, M. 1993 Spectral characteristics of momentum and heat transfer in the turbulent wake of a circular cylinder. *Exp. Therm. Fluid Sci.* **6**, 371–375.

Benzi, R., Succi, S. & Vergassola, M. 1992 Lattice Boltzmann equation: theory and applications. *Phys. Rep.* **222**, 145–197.

Braza, M. 1999 The three-dimensional transition to turbulence in wake flows by means of direct numerical simulation. *Flow Turbul. Combust.* **63**, 315–341.

Chen, S. & Doolen, G. D. 1998 Lattice Boltzmann method for fluid flows. *Annu. Rev. Fluid Mech.* **30**, 329–364.

Djenidi, L. 2006 Lattice Boltzmann simulation of grid-generated turbulence. *J. Fluid Mech.* **552**, 13–35.

Djenidi, L. & Antonia, R. A. 2008 Lattice Boltzmann prediction of three-dimensional natural transition to turbulence. In *Seventeenth Intl Conf. on Discrete Simulation of Fluid Dynamics*, Florianopolis, Brazil.

Djenidi, L. & Moghtaderi, B. 2006 Numerical investigation of laminar mixing in a coaxial microreactor. *J.* Fluid Mech. **568**, 223–242.

Durão, D. F. G, Heitor, M. V. & Pereira, J. C. F. 1988 Measurements of turbulent and periodic flows around a square cross-section cylinder. *Exp. Fluids* **6**, 298–304.

Ezersky, A. B, Lecordier, J. C., Paranthoën, P & Soustov, P. L. 2000 Structure of vortices in a Kármán street behind a heated cylinder. *Phys. Rev.* E **61**, 2107–2110.

Frisch, U., Hasslacher, B. & Pomeau, Y. 1986 Lattice gas automata for the Navier–Stokes equations. *Phys. Rev. Lett.* **56**, 1505–1508.

Godard, G. 2001 Experimental study of a passive scalar field in a Bénard–Kármán street. PhD Thesis, University of Rouen, France.

Godard, G., Weiss, F., Gonzalez, M. & Paranthoën, P. 2005 Heat transfer from a line source located in the periodic laminar near wake of a circular cylinder. *Exp. Therm. Fluid Sci.* **29**, 947–956.

Green, R. B. & Gerrard, J. H. 1991 An optical interferometric study of the wake of a bluff body. *J. Fluid Mech.* **226**, 219–242.

Liou, T.-M., Chen, S.-H., & Hwang, P.-W. 2002 Large eddy simulation of turbulent wake behind a square cylinder with a nearby wall. *J. Fluid Engng* **124**, 81–90.

Massaioli, F., Benzi, R. & Succi, S. 1993 Exponential tails in two-dimensional Rayleigh–Bénard convection. *Europhys. Lett.* **21**, 305–310.

Matsumura, M. & Antonia, R. A. 1993 Momentum and heat transport in the turbulent intermediate wake of a circular cylinder. *J. Fluid Mech.* **250**, 651–668.

Mi, J. & Antonia, R. A. 1993 Thermal characteristics of turbulent vortices in the wake of a circular cylinder. In *Proceedings of the Nineth Symposium on Turbulent Shear Flows*, Kyoto, Japan.

Mi, J. & Antonia, R. A. 1994 Temperature distribution within vortices in the wake of a cylinder. *Intl J. Heat Mass Transfer* **37**, 1048–1050.

Mydlarski, L. & Warhaft, Z. 1998 Passive scalar statistics in high-Péclet-number grid turbulence. *J. Fluid Mech.* **358**, 135–175.

Okude, M. & Matsui, T. 1987*a* Correspondance of velocity fluctuations to flow patterns in a Kármán vortex street at low Reynolds numbers. *Trans. Japan Soc. Aeronaut. Space Sci.* **30** (88), 80–90.

Okude, M. & Matsui, T. 1987*b* Vorticity distribution of vortex street in the wake of a circular cylinder. *Trans. Japan Soc. Aeronaut. Space Sci.* **33** (99), 1–13.

Paranthoën, P., Godard, G., Weiss, F. & Gonzalez, M. 2004 Counter gradient diffusion vs counter diffusion temperature profile. *Intl J. Heat Mass Transfer* **47**, 819–825.

Persillon, H. & Braza, M. 1998 Physical analysis of the transition to turbulence in the wake of a circular cylinder by three-dimensional Navier–Stokes simulation. *J. Fluid Mech.* **365**, 23–88.

Rehab, H., Antonia, R. A., Djenidi, L. & Mi, J. 2000 Characteristics of fluorescein dye and temperature fluctuations in a turbulent near-wake. *Exp. Fluids* **28**, 462–470.

Shadaram, A., Fard, M. A. & Rostamy, N. 2008 Experimental study of near-wake flow behind a rectangular cylinder. *Am. J. Appl. Sci.* **5** (8), 917–926.

Sreenivasan, K. R. 1996 The passive scalar spectrum and the Obukhov–Corrsin constant. *Phys. Fluids* **8**, 189–196.

Succi, S. 2001 The lattice Boltzmann equation for fluid dynamics and Beyond. *Numer. Math. Sci. Comput*. Oxford University Press.

Warhaft, Z. 2000 Passive scalar in turbulent flows. *Annu. Rev. Fluid Mech.* **32**, 203–240.

Watanabe, T. & Gotoh, T. 2004 Statistics of a passive scalar in homogeneous turbulence. *New J. Phys* **6**, 40 (http://www.njp.org/).

Williamsom, C. H. K. 1996*a* Vortex dynamics in the cylinder wake. *Annu. Rev. Fluid Mech.* **28**, 477–539.

Williamsom, C. H. K. 1996*b* Three-dimensional wake transition. *J. Fluid Mech.* **328**, 345–407.

Yuan, P. & Schaefer, L. 2006 A thermal lattice Boltzmann two-phase flow model and its application to heat transfer problems. Part 1. Theoretical foundation, *J. Fluid Engng* **128**, 142–150.